

Nicola de Divitiis

# Lyapunov Analysis for Fully Developed Homogeneous Isotropic Turbulence

Received: date / Accepted: date

**Abstract** The present work studies the isotropic and homogeneous turbulence for incompressible fluids through a specific Lyapunov analysis, assuming that the turbulence is due to the bifurcations associated to the velocity field.

The analysis consists in the calculation of the velocity fluctuation through the Lyapunov analysis of the local deformation and the Navier-Stokes equations and in the study of the mechanism of the energy cascade from large to small scales through the finite scale Lyapunov analysis of the relative motion between two particles.

The analysis provides an explanation for the mechanism of the energy cascade, leads to the closure of the von Kármán-Howarth equation, and describes the statistics of the velocity difference.

Several tests and numerical results are presented.

**Keywords** Bifurcations · Lyapunov Analysis · von Kármán-Howarth equation · Velocity difference statistics

**PACS** 47.27.-i

## 1 Introduction

In this work a novel procedure based on a specific Lyapunov analysis is presented for studying the incompressible isotropic and homogeneous turbulence in an infinite domain. The analysis is mainly motivated by the fact that in turbulence the kinematics of the fluid deformation is subjected to bifurcations [1] and exhibits a chaotic behavior and huge mixing [2], [3], resulting to be much more rapid than the fluid state variables. This characteristics implies that the accepted kinematical hypothesis for deriving the Navier-Stokes equations could require the consideration of very small length scales and times for describing the fluid motion [4] and therefore a very large number of degrees of freedom.

As well known, other peculiar characteristics of the turbulence are the mechanism of the kinetic energy cascade, directly related to the relative motion of a pair of fluid particles [5], [6], [7], [8] and responsible for the shape of the developed energy spectrum, and the non-gaussian statistics of the velocity difference.

The present analysis assumes that the fluctuations of all the fluid state variables are the result of the bifurcations of the velocity field.

In the first part of the work, the velocity fluctuation is studied through the kinematics of the local deformation and the momentum equations. These momentum equations are expressed with respect to

the referential coordinates which coincide with the material coordinates for a given fluid configuration [4], whereas the kinematics of the local deformation is analyzed with the Lyapunov theory. The choice of the referential coordinates allows the velocity fluctuations to be analytically expressed in terms of the Lyapunov exponent of the local fluid deformation.

The second part deals with the study of velocity difference between two fixed points of the space. This is analyzed with an opportune finite scale Lyapunov theory studying the motion of the particles crossing the two points, in the finite scale Lyapunov basis. This analysis postulates that the motion of the Lyapunov basis and that of the fluid with respect to the same basis, are completely statistically uncorrelated. This crucial assumption arises from the condition of fully developed turbulence. The study leads to the closure of the von Kármán-Howarth equation [7] and gives an explanation of the mechanism of kinetic energy transfer between length scales. The obtained expression of the function  $K(r)$ , which represents the inertia forces, is in terms of the longitudinal correlation function and its spatial derivative, and satisfies the conservation law which states that the inertia forces only transfer the kinetic energy [7], [8].

Furthermore, the statistics of velocity difference is studied with the Fourier analysis of the velocity fluctuations, and an analytical expression for the velocity difference and for its PDF is obtained in case of isotropic turbulence. This expression incorporates an unknown function, related to the skewness, which is identified through the obtained expression of  $K(r)$ . The velocity difference also requires the knowledge of the critical Reynolds number whose estimation is made in the Appendix B, where the order of magnitude is roughly determined through a qualitative analysis of the bifurcations of the velocity field.

Finally, the several results obtained with this analysis are compared with the data existing in the literature, indicating that the proposed analysis can adequately describe the various properties of the fully developed turbulence.

The present analysis only studies the possibility to obtain the fully developed homogeneous-isotropic turbulence in a given condition and does not analyze the intermediate stages of the turbulence.

## 2 Lyapunov analysis of velocity fluctuation

In this section, the velocity fluctuation, due to the bifurcations of the velocity field, is calculated through the Lyapunov analysis of the kinematic of velocity field, using the Navier-Stokes equations.

Starting from the momentum Navier-Stokes equations written in a frame of reference  $\mathfrak{R}$

$$\frac{\partial u_k}{\partial t} = -\frac{\partial u_k}{\partial x_h} u_h + \frac{1}{\rho} \frac{\partial T_{kh}}{\partial x_h} \quad (1)$$

consider the map  $\chi : \mathbf{x}_0 \rightarrow \mathbf{x}$ , which is the function that determines the current position  $\mathbf{x}$  of a fluid particle located at the referential position  $\mathbf{x}_0$  [4] at  $t = t_0$ . Equation (1) can be written in terms of the referential position  $\mathbf{x}_0$  [4]

$$\frac{\partial u_k}{\partial t} = \left( -\frac{\partial u_k}{\partial x_{0p}} u_h + \frac{1}{\rho} \frac{\partial T_{kh}}{\partial x_{0p}} \right) \frac{\partial x_{0p}}{\partial x_h} \quad (2)$$

The Lyapunov analysis of the fluid strain provides the expression of this deformation in terms of the maximal Lyapunov exponent

$$\frac{\partial \mathbf{x}}{\partial \mathbf{x}_0} \approx e^{\Lambda(t-t_0)} \quad (3)$$

where  $\Lambda = \max(\Lambda_1, \Lambda_2, \Lambda_3)$  is the maximal Lyapunov exponent and  $\Lambda_i$ , ( $i = 1, 2, 3$ ) are the Lyapunov exponents. Due to the incompressibility,  $\Lambda_1 + \Lambda_2 + \Lambda_3 = 0$ , thus,  $\Lambda > 0$ .

The momentum equations written using the referential coordinates allow the factorization of the velocity fluctuation and to express it in Lyapunov exponential form of the local fluid deformation.

If we assume that this deformation is much more rapid than  $\partial T_{kh}/\partial x_{0p}$  and  $\partial u_k/\partial x_{0p} u_h$ , the velocity fluctuation can be obtained from Eq. (2), where  $\partial T_{kh}/\partial x_{0p}$  and  $\partial u_k/\partial x_{0p} u_h$  are supposed to be constant with respect to the time

$$u_k \approx \frac{1}{\Lambda} \left( -\frac{\partial u_k}{\partial x_{0p}} u_h + \frac{1}{\rho} \frac{\partial T_{kh}}{\partial x_{0p}} \right)_{t=t_0} \approx \frac{1}{\Lambda} \left( \frac{\partial u_k}{\partial t} \right)_{t=t_0} \quad (4)$$

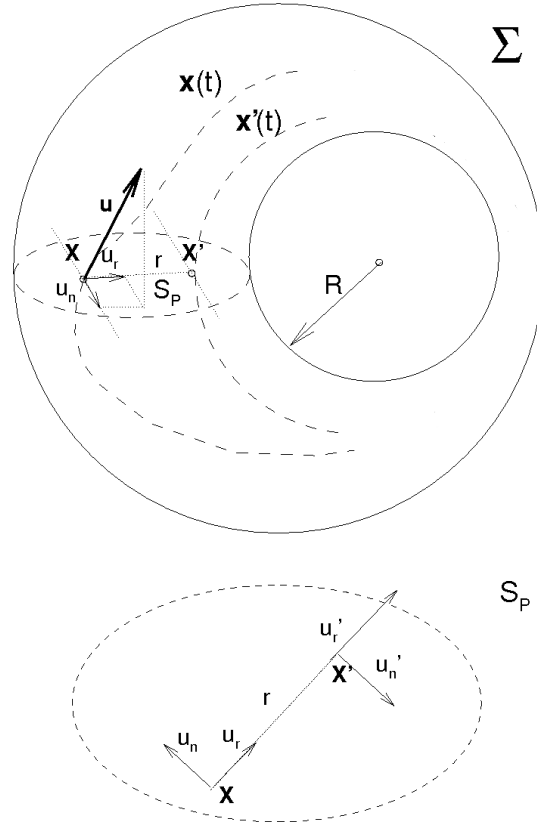


**Fig. 1** Scheme of the relative motion of two fluid particles

This assumption is justified by the fact that, according to Truesdell [4],  $\partial T_{kh}/\partial x_{0p} - \partial u_k/\partial x_{0p} u_h$  is a smooth function of time -at least during the period of a fluctuation- whereas the fluid deformation varies very rapidly in proximity of a bifurcation according to Eq. (3). This implies that, in proximity of bifurcations, the Lyapunov basis of orthonormal vectors  $E_A \equiv (\mathbf{e}'_1, \mathbf{e}'_2, \mathbf{e}'_3)$  [10] associated to the strain (3) rotates very quickly with respect to  $\mathfrak{R}$  with an angular velocity  $\omega_A$ , whereas the fluid velocity fluctuation, measured in  $E_A$  results to be a quantity whose modulus increases with a rate  $\approx e^{\Lambda(t-t_0)}$ . Since  $\Lambda$  is related to the maximal eigenvalue of  $(\nabla \mathbf{u} + \nabla \mathbf{u}^T)/2$ , according to the fluid kinematics [2], [3], [9]  $|\omega_A| = O(\Lambda)$ . Therefore, the fluid velocity fluctuation measured in  $\mathfrak{R}$ , varies very quickly because of the combined effect of the exponential growth rate and of the rotations of  $E_A$  with respect to  $\mathfrak{R}$ .

### 3 Lyapunov analysis of the relative motion

In order to investigate the mechanism of the energy cascade, the properties of the relative motion are now studied with the Lyapunov analysis of the equations of motion between fluid particles. To this purpose, consider two fixed points of the space,  $\mathbf{X}$  and  $\mathbf{X}'$  (see Fig. 1) with  $\mathbf{r} = \mathbf{X}' - \mathbf{X}$ , where  $r = |\mathbf{r}|$  is the separation distance, and the motion of two fluid particles which at a given time  $t_0$ , cross through  $\mathbf{X}$  and  $\mathbf{X}'$ . The equations of motion of these particles are

$$\frac{d\mathbf{x}}{dt} = \mathbf{u}(\mathbf{x}, t), \quad \frac{d\mathbf{x}'}{dt} = \mathbf{u}(\mathbf{x}', t) \quad (5)$$

$\hat{\mathbf{r}} = \mathbf{x}' - \mathbf{x}$  represents the relative position between the two particles, therefore  $\hat{\mathbf{r}}(t_0) = \mathbf{r}$ . The fluctuations of the velocity field are supposed to be caused of the bifurcations of Eqs. (5).

The Lyapunov analysis of Eqs. (5) leads to the determination of the maximal finite scale Lyapunov exponent  $\lambda$  associated to Eqs. (5)

$$\lambda(r) = \lim_{T \rightarrow \infty} \frac{1}{T} \int_0^T \frac{(\mathbf{u}(\mathbf{x}') - \mathbf{u}(\mathbf{x})) \cdot (\mathbf{x}' - \mathbf{x})}{(\mathbf{x}' - \mathbf{x}) \cdot (\mathbf{x}' - \mathbf{x})} dt \quad (6)$$

where  $\lambda(0) = \Lambda$ , and the separation distance  $r$  represents the scale associated to  $\lambda$ . Now, we define the finite scale Lyapunov basis associated to Eqs. (5) as well as in the case of the standard Lyapunov vectors [10]. Then, consider the system

$$\begin{aligned} \frac{d\mathbf{x}}{dt} &= \mathbf{u}(\mathbf{x}, t), \\ \frac{d\hat{\mathbf{r}}}{dt} &= \mathbf{u}(\mathbf{x} + \hat{\mathbf{r}}, t) - \mathbf{u}(\mathbf{x}, t) \end{aligned} \quad (7)$$

and introduce the Lyapunov vectors  $\mathbf{r}_1$ ,  $\mathbf{r}_2$  and  $\mathbf{r}_3$  which satisfy Eqs. (7). The finite scale Lyapunov basis  $E_\lambda \equiv (\mathbf{e}_1, \mathbf{e}_2, \mathbf{e}_3)$  of Eqs. (5) is obtained by orthogonalizing  $\mathbf{r}_1$ ,  $\mathbf{r}_2$  and  $\mathbf{r}_3$  with the Gram-Schmidt method at each time [10]. This basis rotates with respect to  $\mathfrak{R}$  with an angular velocity equal to  $-\boldsymbol{\omega}_\lambda$ , and the fluid velocity difference  $\Delta\mathbf{v}$  measured in  $E_\lambda$  is expressed by the Lyapunov theory as

$$v'_l - v_l = \lambda_l \hat{r}_l, \quad l = 1, 2, 3 \quad (8)$$

Into Eq. (8),  $\lambda_l$  is the Lyapunov exponent associated to the direction  $\hat{r}_l$ , where  $\hat{r}_l$ ,  $v_l$  and  $v'_l$  are, respectively, the components of  $\mathbf{x}' - \mathbf{x}$  and the components of  $\mathbf{u}(\mathbf{X}, t)$  and  $\mathbf{u}(\mathbf{X}', t)$  measured in  $E_\lambda$ .  $\Delta\mathbf{v} \equiv (v'_1 - v_1, v'_2 - v_2, v'_3 - v_3)$  can be also written in terms of the maximal exponent  $\lambda$

$$\Delta\mathbf{v}(\hat{\mathbf{r}}) = \lambda(r)\hat{\mathbf{r}} + \boldsymbol{\zeta} \quad (9)$$

where  $\boldsymbol{\zeta}$ , due to the other two exponents, is negligible with respect to  $\lambda\mathbf{r}$  and makes  $\Delta\mathbf{v}(r)$  a solenoidal field, resulting  $|\boldsymbol{\zeta}| \ll |\lambda\mathbf{r}|$  during the fluctuation. When  $\boldsymbol{\zeta}/\lambda r \rightarrow 0$ ,  $\hat{\mathbf{r}}$  exhibits unaltered orientation with respect to  $E_\lambda$ . The velocity difference  $\Delta\mathbf{u}$ , measured in  $\mathfrak{R}$  and expressed in  $E_\lambda$ , calculated when  $|\hat{\mathbf{r}}| = r$ , is

$$\Delta\mathbf{u}(\hat{\mathbf{r}}) = \lambda(r)\hat{\mathbf{r}} + \boldsymbol{\zeta} + \boldsymbol{\omega}_\lambda \times \hat{\mathbf{r}} \quad (10)$$

This equation states that the angular velocity  $\boldsymbol{\omega}_\lambda$  determines the lateral components of the velocity difference in  $E_\lambda$  and, because of isotropy, its modulus is proportional to  $\lambda(r)$ . Although  $\boldsymbol{\omega}_\lambda$  and  $\Delta\mathbf{v}$  arise from Eq. (7), these are not directly related, therefore, we suppose here that  $\boldsymbol{\omega}_\lambda$  is statistically orthogonal to both  $\mathbf{v}$  and  $\mathbf{v}'$ , with  $\langle \boldsymbol{\omega}_\lambda \rangle = 0$ . This is the crucial assumption of the present work which is justified by the condition of fully developed turbulence. This provides that

$$\langle \boldsymbol{\omega}_\lambda v_p^m v_q'^n \rangle = 0, \quad m > 0, \quad n > 0, \quad p, q = 1, 2, 3, \quad (11)$$

where the angular brackets denote the average calculated on the statistical ensemble of all the pairs of particles which cross through  $\mathbf{X}$  and  $\mathbf{X}'$ . Again, thanks to the fully developed turbulence, we suppose that the orientation of  $E_\lambda$  with respect to  $\mathfrak{R}$  and  $\boldsymbol{\omega}_\lambda$  are statistically orthogonal each other, i.e.

$$\langle \omega_{\lambda p}^m e_q^n \rangle = \langle \omega_{\lambda p}^m \rangle \langle e_q^n \rangle, \quad m > 0, \quad n > 0, \quad p, q = 1, 2, 3, \quad (12)$$

where  $\boldsymbol{\omega}_\lambda \equiv (\omega_{\lambda 1}, \omega_{\lambda 2}, \omega_{\lambda 3})$ , and  $e_{ip}$  represents the component of  $\mathbf{e}_i$  along the direction  $p$  in  $\mathfrak{R}$ . Due to isotropy, we also assume that

$$\langle \omega_{\lambda h} \omega_{\lambda k} \rangle = \frac{1}{3} \langle \boldsymbol{\omega}_\lambda \cdot \boldsymbol{\omega}_\lambda \rangle \delta_{hk}, \quad \langle e_{hp} e_{kq} \rangle = \frac{1}{3} \delta_{hk} \delta_{pq} \quad (13)$$

and

$$\langle \omega_{\lambda i}^2 \rangle = a_i \lambda^2(r), \quad i = 1, 2, 3 \quad (14)$$

where  $a_i = O(1)$  do not depend on  $r$ .

Under these hypothesis, we now show the following equations

$$\langle u_r u'_r \omega_{\lambda k} \rangle = 0 \quad (15)$$

$$\langle u_n u'_n \omega_{\lambda k} \rangle = \langle u_b u'_b \omega_{\lambda k} \rangle = C_k u^2 \lambda(r) g(r) \quad (16)$$

where  $u_r$ ,  $u_n$  and  $u_b$  are the components of  $\mathbf{u}$  along  $\hat{\mathbf{r}}$  and along its two orthogonal direction  $n$  and  $b$ , and  $C_k$  is a proper constant of the order of unity. The function  $g(r) = \langle u_n u'_n \rangle / u^2$  and  $u^2 = \langle u_i u_i \rangle / 3$  are, respectively, the lateral velocity correlation function and the standard deviation of the longitudinal

velocity (see Appendix A). This correlation function measured in  $E_\lambda$ , due to the isotropy, is equal to that which measured in  $\mathfrak{R}$ .

Equation (15) is the direct consequence of Eq. (11). In fact  $\langle u_r u'_r \omega_\lambda \rangle \equiv \langle v_r v'_r \omega_\lambda \rangle = 0$ .

To demonstrate Eq. (16), observe that  $u_n$  and  $\omega_\lambda$  can be decomposed into  $n$  independent, identically distributed, stochastic variables  $\xi_k$ , which satisfy [12]

$$\langle \xi_k \rangle = 0, \quad \langle \xi_h \xi_k \rangle = \delta_{hk} \quad \langle \xi_h \xi_k \xi_l \rangle = \varpi_{hkl} q \quad (17)$$

where  $\varpi_{hkl} = 1$  if  $h = k = l$ , else  $\varpi_{hkl} = 0$  and  $q \neq 0$ . Thanks to Eq. (14),  $\omega_{\lambda j}$  is expressed as the sum of  $\xi_k$ , where the coefficients of the combination are constant with respect to  $\mathbf{X}$  and equal each other [12].

$$\omega_{\lambda j} = A_j \lambda(r) \frac{1}{n} \sum_{k=1}^n \xi_k \quad (18)$$

with  $A_1 = A_2 = A_3 = O(1)$  constant parameters. The component  $u_n$  (and  $u_b$ ) depends on  $\mathbf{X}$  and is expressed as the linear combination of  $\xi_k$  whose coefficients are functions of  $\mathbf{X}$ , i.e.

$$u_n(\mathbf{X}) = u \sum_{k=1}^n F_k(\mathbf{X}) \xi_k \quad (19)$$

Hence, the correlation function  $g(r)$  is in terms of  $F_k$  and is determined through Eq. (19) and (17) [12], putting  $\mathbf{X} = 0$ .

$$g(r) = \sum_{k=1}^n F_k(0) F_k(\mathbf{r}) \quad (20)$$

Therefore,  $\langle u_n u'_n \omega_{\lambda k} \rangle$  is calculated taking into account Eq. (18), (19), (20) and (17), and, as a result, Eq. (16) is achieved.

#### 4 Closure of the von Kármán-Howarth equation

Now, we propose the closure of the von Kármán-Howarth equation based on the analysis seen at the previous section.

The term representing the inertia forces in the von Kármán-Howarth equation is expressed by Eq. (68) (see Appendix A), and is [7], [8]

$$\frac{\partial}{\partial \hat{r}_k} (\hat{r}_k K(r)) = \frac{\partial}{\partial \hat{r}_k} \langle u_i u'_i (u_k - u'_k) \rangle \quad (21)$$

where, due to isotropy  $K$  is a function of  $r$  alone [7].

Equation (21) is the divergence of  $\hat{\mathbf{r}} K(r)$  and gives the mechanism of energy transfer between scales which does not depend upon the frame of reference [7] [8]. In order to obtain  $K(r)$ , Eq. (21) is here written in  $E_\lambda$ . In view of Eq. (8) and taking into account that  $u_i u'_i$  is also frame independent, one obtains the following equation

$$\frac{\partial}{\partial \hat{r}_k} (\hat{r}_k K(r)) = -\frac{\partial}{\partial \hat{r}_k} (\langle u_i u'_i \lambda \rangle \hat{r}_k + (\langle u_i u'_i \omega_\lambda \rangle \times \hat{\mathbf{r}})_k + \langle u_i u'_i \zeta_k \rangle) \quad (22)$$

from which one determines the general expression for of  $K(r)$ . Since  $\lambda$  is calculated with Eq. (6), this is constant with respect to the statistics of  $u_i$  and  $u'_i$ , thus  $\langle \lambda u_i u'_i \rangle = \lambda \langle u_i u'_i \rangle$ , and  $K(r)$  is expressed as the general integral of Eq. (22)

$$K(r) \hat{\mathbf{r}} = -\lambda \langle u_i u'_i \rangle \hat{\mathbf{r}} - \langle u_i u'_i \omega_\lambda \rangle \times \hat{\mathbf{r}} + \mathbf{s} \quad (23)$$

Into Eq. (23),  $\mathbf{s}$  is the sum of a term due to  $\zeta$  plus an arbitrary solenoidal field arising from the integration of Eq. (22) [13]. According to this analysis of Lyapunov,  $\mathbf{s}$  is proportional to  $u^2 \lambda r$  and can be written in the form

$$\mathbf{s} = u^2 \lambda(r) r \mathbf{s}_0 \quad (24)$$

Substituting Eq. (64) (see Appendix A) and Eq. (24) into Eq. (23), one obtains

$$K(r)\hat{\mathbf{r}} = (\lambda u^2(g - f) - 3\lambda u^2 g)\hat{\mathbf{r}} - \langle u_i u'_i \boldsymbol{\omega}_\lambda \rangle \times \hat{\mathbf{r}} + u^2 \lambda(r) r \mathbf{s}_0 \quad (25)$$

where  $f(r)$  is the longitudinal velocity correlation functions.

Equation (25) is made by three addends. In the first one of these, the part into the brackets is an even function of  $r$  which goes to zero as  $r \rightarrow \infty$  and assumes the value  $-3u^2\lambda(0)$  for  $r = 0$ . The second term, orthogonal to the first one, vanishes at  $r = 0$  and tends to zero when  $r \rightarrow \infty$ . In this latter  $u_i u'_i$  is expressed in  $E_\lambda$  for sake of convenience

$$\langle u_i u'_i \boldsymbol{\omega}_\lambda \rangle = \langle u_r u'_r \boldsymbol{\omega}_\lambda \rangle + \langle u_n u'_n \boldsymbol{\omega}_\lambda \rangle + \langle u_b u'_b \boldsymbol{\omega}_\lambda \rangle \quad (26)$$

The first term at the RHS of Eq. (26) vanishes because of Eq. (15), whereas the other ones are expressed by means of Eq. (16). Therefore

$$\langle u_i u'_i \boldsymbol{\omega}_\lambda \rangle \times \hat{\mathbf{r}} = 2u^2 \lambda(r) g(r) \mathbf{c} \times \hat{\mathbf{r}} \quad (27)$$

where  $\mathbf{c} \equiv (C_1, C_2, C_3)$  and  $C_k = O(1)$  are from Eq. (16).

In order to satisfy Eq. (25), the expression of  $\mathbf{s}_0$  must be of the kind  $\mathbf{s}_0 = h(r)\hat{\mathbf{t}} + p(r)\mathbf{n}$ , where, according to Ref. [8],  $h(r)$  and  $p(r)$  are even functions of  $r$ , that due to isotropy,  $h(r) = p(r)$ , and  $\mathbf{s}_0$  is

$$\mathbf{s}_0 = h(r)(\mathbf{t} + \mathbf{n}) \quad (28)$$

where  $\mathbf{t} = \hat{\mathbf{r}}/r$ ,  $\mathbf{n} = (\mathbf{c} \times \hat{\mathbf{r}})/|\mathbf{c} \times \hat{\mathbf{r}}|$ .

To determine  $K(r)$  and  $h(r)$ , Eq. (23) is projected along the directions  $\hat{\mathbf{r}}$  and  $\mathbf{n}$

$$K(r) = \lambda u^2(g - f) - 3u^2 \lambda g + \frac{\mathbf{s} \cdot \hat{\mathbf{r}}}{r^2} \quad (29)$$

$$\mathbf{s} \cdot \mathbf{n} = \langle u_i u'_i \boldsymbol{\omega}_\lambda \times \hat{\mathbf{r}} \rangle \cdot \mathbf{n} \quad (30)$$

From Eq. (30)

$$h(r) = Hg(r) \quad (31)$$

where  $H = 2(\mathbf{c} \times \hat{\mathbf{r}}) \cdot \mathbf{n}/r = O(1)$ . As  $\zeta/r \rightarrow 0$ ,  $\hat{\mathbf{r}}$  maintains the same orientation in  $E_\lambda$ , thus  $H$  is an invariant which has to be identified. The function  $K(r)$  is determined with Eq. (29)

$$K(r) = \lambda u^2(g - f) + u^2 \lambda(r) g(r)(H - 3) \quad (32)$$

$K(r)$  satisfies the conditions  $\partial K(0)/\partial r = 0$  and  $K(0) = 0$  [8], which represent, respectively, the homogeneity of the flow and the condition that the inertia forces do not modify the fluid kinetic energy. Since  $g(0) = f(0) = 1$ , this immediately identifies  $H = 3$  and

$$K(r) = \lambda u^2 (g - f) \quad (33)$$

Due to the fluid incompressibility,  $f$  and  $g$  are related each other through  $g = f + 1/2 \partial f / \partial r r$  (see Eq. (66), Appendix A), leading to the expression

$$K(r) = \frac{1}{2} u^2 \frac{\partial f}{\partial r} \lambda(r) r \quad (34)$$

This expression of  $K(r)$  has been obtained studying the properties of velocity difference in  $E_\lambda$ .

Equation (34) states that, the fluid incompressibility, expressed by  $g - f \neq 0$ , represents a sufficient condition to state that  $K(r) \neq 0$ . This latter is determined as soon as  $\lambda$  is known. To calculate  $\lambda$ , it is convenient to express  $\Delta \mathbf{u} = \mathbf{u}(\mathbf{x}', t) - \mathbf{u}(\mathbf{x}, t)$  in  $\mathfrak{R}$ , with  $\hat{\mathbf{r}} = (r, 0, 0)$ . Then,  $\Delta u_r$  can be expressed in terms of  $\hat{\mathbf{r}}$  and  $\Delta \mathbf{v}$  as

$$\Delta u_r = \boldsymbol{\xi} \cdot \mathbf{Q} \Delta \mathbf{u} \quad (35)$$

Into Eqs. (35),  $\mathbf{Q} \equiv ((e_{ij}))$  is the rotation matrix transformation from  $E_\lambda$  to  $\mathfrak{R}$ , where  $e_{ij}$  is the component of  $\mathbf{e}_j$  along the coordinate direction  $i$  on  $\mathfrak{R}$ , and  $\boldsymbol{\xi} = (\mathbf{X}' - \mathbf{X})/|\mathbf{X}' - \mathbf{X}| \equiv (1, 0, 0)$ .

The standard deviation of  $\Delta u_r$  is calculated from Eqs. (35), assuming  $\zeta = 0$ , i.e.  $\Delta \mathbf{u} = \lambda \hat{\mathbf{r}} + \boldsymbol{\omega}_\lambda \times \hat{\mathbf{r}}$  and that  $\mathbf{Q}$  and  $\boldsymbol{\omega}_\lambda$  are fluctuating depending on the pair paths with  $\langle \boldsymbol{\omega}_\lambda \rangle = 0$ :

$$\begin{aligned} \langle (\Delta u_r)^2 \rangle &= \sum_{i,j,k,l} \sum_{p,q,r,s} (\xi_i \xi_p \langle \lambda^2 e_{ij} e_{pq} \rangle \hat{r}_j \hat{r}_q + \xi_i \xi_p \langle \lambda e_{ij} e_{pq} \omega_{\lambda r} \rangle \hat{r}_j \hat{r}_s \varepsilon_{qrs} + \xi_i \xi_p \langle \lambda e_{ij} e_{pq} \omega_{\lambda k} \rangle \hat{r}_q \hat{r}_l \varepsilon_{jkl} + \\ &\quad \xi_i \xi_p \langle e_{ij} e_{pq} \omega_{\lambda k} \omega_{\lambda r} \rangle \hat{r}_l \hat{r}_s) \varepsilon_{jkl} \varepsilon_{qrs} \end{aligned} \quad (36)$$

where  $\boldsymbol{\xi} \equiv (\xi_1, \xi_2, \xi_3)$  and  $\varepsilon_{ijk} = (j-i)(k-i)(k-j)/2$  is the Levi-Civita epsilon arising from the cross product.

Since  $\lambda$  is calculated as the average of the velocity increment per unit distance, it is constant with respect the statistics of  $\mathbf{Q}$  and  $\boldsymbol{\omega}_\lambda$ , thus  $\langle \lambda^2 \dots \rangle = \lambda^2 \langle \dots \rangle$ . Although  $\mathbf{Q}$  and  $\boldsymbol{\omega}_\lambda$  are related by the definition of angular velocity, due to Eq. (12), these are statistically independent, so that  $\langle e_{ij} e_{pq} \omega_{\lambda k} \rangle = \langle e_{ij} e_{pq} \rangle \langle \omega_{\lambda k} \rangle = 0$  and  $\langle e_{ij} e_{pq} \omega_{\lambda k} \omega_{\lambda r} \rangle = \langle e_{ij} e_{pq} \rangle \langle \omega_{\lambda k} \omega_{\lambda r} \rangle$ , therefore second and third terms vanish into Eq. (36).

Due to the isotropy, the Lyapunov basis satisfies Eq. (13) ( $\langle e_{ij} e_{pq} \rangle = \delta_{ip} \delta_{jq} / 3$ ). This is introduced in the first term of Eq. (36), which thus depends on  $r^2$  alone. This term, which equals  $\lambda^2 r^2 / 3$ , is associated to the direction  $\hat{\mathbf{r}}$  (maximal Lyapunov exponent direction) and represents one degree of freedom in the space. Again thanks to the isotropy, the last term of Eq. (36) is two times the first one because it is caused by  $\boldsymbol{\omega}_\lambda$  which corresponds to the two directions orthogonal to  $\hat{\mathbf{r}}$  and thus to two degrees of freedom. As a result, taking into account that  $\varepsilon_{ijk} \varepsilon_{ijh} = 2\delta_{hk}$ , the standard deviation of the longitudinal velocity difference is

$$\langle (\Delta u_r)^2 \rangle = \lambda^2 r^2 \quad (37)$$

with

$$\lambda(r) = \sqrt{\frac{\langle \boldsymbol{\omega}_\lambda \cdot \boldsymbol{\omega}_\lambda \rangle}{3}} \quad (38)$$

This standard deviation can be expressed through the longitudinal correlation function  $f$

$$\langle (\Delta u_r)^2 \rangle = 2u^2(1 - f(r)) \quad (39)$$

being  $u$  the standard deviation of the longitudinal velocity. The maximal Lyapunov exponent is calculated in function of  $f$ , from Eqs. (37) and (39)

$$\lambda(r) = \frac{u}{r} \sqrt{2(1 - f(r))} \quad (40)$$

Hence, substituting Eq. (40) into Eq. (34), one obtains the expression of  $K(r)$  in terms of the longitudinal correlation function

$$K(r) = u^3 \sqrt{\frac{1-f}{2}} \frac{\partial f}{\partial r} \quad (41)$$

Equation (41) represents the proposed closure of the von Kármán-Howarth equation. This corresponds to a mechanism of the kinetic energy transferring between diverse regions of space which preserves the average values of the momentum and of the kinetic energy. Specifically, the analytical structure of Eq.(41) states that this mechanism consists of a flow of the kinetic energy from large to small scales which only redistributes the kinetic energy between wavelengths.

This mechanism can be interpreted as follows. If, at  $t_0$ , a toroidal volume  $\Sigma(t_0)$  is taken which contains  $\mathbf{X}$  and  $\mathbf{X}'$  (see Fig. 1), its geometry and position change according to the fluid motion, and its dimensions,  $\sqrt{S_p}$  and  $R$ , vary with time to preserve the volume. Choosing  $\Sigma$  in such a way that  $R$  increases with time, the Lyapunov analysis of Eqs. (5) leads to  $R \approx R(t_0) e^{\lambda(t-t_0)}$ . According to the theory [11], for  $t > t_0$ , the trajectories of the two particles are enclosed into  $\Sigma(t)$ . Hence, the kinetic energy, initially enclosed into  $\Sigma(t_0)$ , at the end of the fluctuation is contained into  $\Sigma(t)$  whose dimensions are changed with respect to  $\Sigma(t_0)$ . The kinetic energy is then transferred far from  $\mathbf{X}$  and  $\mathbf{X}'$ , resulting enclosed in a more thin toroid.

## 5 Skewness of velocity difference PDF

The obtained expression of  $K(r)$  allows to determine the skewness of  $\Delta u_r$  [8]

$$H_3(r) = \frac{\langle (\Delta u_r)^3 \rangle}{\langle (\Delta u_r)^2 \rangle^{3/2}} = \frac{6k(r)}{(2(1 - f(r)))^{3/2}} \quad (42)$$

which is expressed in terms of the longitudinal triple correlation  $k(r)$ , linked to  $K(r)$  by  $K(r) = u^3 (\partial/\partial r + 4/r) k(r)$  (also see Appendix A, Eq. (69)). Since  $f$  and  $k$  are, respectively, even and odd functions of  $r$  with  $f(0) = 1$ ,  $k(0) = k'(0) = k''(0) = 0$ ,  $H_3(0)$  is given by

$$H_3(0) = \lim_{r \rightarrow 0} H_3(r) = \frac{k'''(0)}{(-f''(0))^{3/2}} \quad (43)$$

where the apex denote the derivative with respect to  $r$ . To obtain  $H_3(0)$ , observe that, near the origin,  $K$  behaves as

$$K = u^3 \sqrt{-f''(0)} f''(0) \frac{r^2}{2} + O(r^4) \quad (44)$$

then, substituting Eq. (44) into  $K(r) = u^3 (\partial/\partial r + 4/r) k(r)$  and accounting for Eq. (43), one obtains

$$H_3(0) = -\frac{3}{7} = -0.42857... \quad (45)$$

This value of  $H_3(0)$  is a constant of the present analysis, which does not depend on the Reynolds number. This is in agreement with the several sources of data existing in the literature such as [8], [14], [15], [16] (and Refs. therein) and its value gives the entity of the mechanism of energy cascade.

## 6 Statistical analysis of velocity difference

As explained in this section, the Lyapunov analysis of the local deformation and some plausible assumptions about the statistics of velocity difference  $\Delta \mathbf{u}(\mathbf{r}) \equiv \mathbf{u}(\mathbf{X} + \mathbf{r}) - \mathbf{u}(\mathbf{X})$  lead to determine all the statistical moments of  $\Delta \mathbf{u}(\mathbf{r})$  with only the knowledge of the function  $K(r)$  and of the value of the critical Reynolds number.

The statistical properties of  $\Delta \mathbf{u}(\mathbf{r})$ , are investigated expressing the velocity fluctuation, given by Eq. (4), as the Fourier series

$$\mathbf{u} \approx \frac{1}{\Lambda} \sum_{\boldsymbol{\kappa}} \frac{\partial \mathbf{U}}{\partial t}(\boldsymbol{\kappa}) e^{i\boldsymbol{\kappa} \cdot \mathbf{x}} \quad (46)$$

where  $\mathbf{U}(\boldsymbol{\kappa}) \equiv (U_1(\boldsymbol{\kappa}), U_2(\boldsymbol{\kappa}), U_3(\boldsymbol{\kappa}))$  are the components of velocity spectrum, which satisfy the Fourier transformed Navier-Stokes equations [8]

$$\frac{\partial U_p(\boldsymbol{\kappa})}{\partial t} = -\nu k^2 U_p(\boldsymbol{\kappa}) + i \sum_{\mathbf{j}} \left( \frac{\kappa_p \kappa_q \kappa_r}{\kappa^2} U_q(\mathbf{j}) U_r(\boldsymbol{\kappa} - \mathbf{j}) - \kappa_q U_q(\mathbf{j}) U_p(\boldsymbol{\kappa} - \mathbf{j}) \right) \quad (47)$$

All the components  $\mathbf{U}(\boldsymbol{\kappa}) \approx \partial \mathbf{U}(\boldsymbol{\kappa}) / \partial t / \Lambda$  are random variables distributed according to certain distribution functions, which are statistically orthogonal each other [8].

Thanks to the local isotropy,  $\mathbf{u}$  is sum of several dependent random variables which are identically distributed [8], therefore  $\mathbf{u}$  tends to a gaussian variable [12], and  $\mathbf{U}(\boldsymbol{\kappa})$  satisfies the Lindeberg condition, a very general necessary and sufficient condition for satisfying the central limit theorem [12]. This condition does not apply to the Fourier coefficients of  $\Delta \mathbf{u}$ . In fact, since  $\Delta \mathbf{u}$  is the difference between two dependent gaussian variables, its PDF could be a non gaussian distribution function. In  $\mathbf{x} = 0$ , the velocity difference  $\Delta \mathbf{u}(\mathbf{r}) \equiv (\Delta u_1, \Delta u_2, \Delta u_3)$  is given by

$$\Delta u_p \approx \frac{1}{\Lambda} \sum_{\boldsymbol{\kappa}} \frac{\partial U_p(\boldsymbol{\kappa})}{\partial t} (e^{i\boldsymbol{\kappa} \cdot \mathbf{r}} - 1) \equiv L + B + P + N \quad (48)$$

This fluctuation consists of the contributions appearing into Eq. (47): in particular,  $L$  represents the sum of all linear terms due to the viscosity and  $B$  is the sum of all bilinear terms arising from inertia and pressure forces.  $P$  and  $N$  are, respectively, the sums of definite positive and negative square terms, which derive from inertia and pressure forces. The quantity  $L + B$  tends to a gaussian random variable being the sum of statistically orthogonal terms [17], [12], while  $P$  and  $N$  do not, as they are linear combinations of squares [17]. Their general expressions are [17]

$$P = P_0 + \eta_1 + \eta_2^2 \quad (49)$$

$$N = N_0 + \zeta_1 + \zeta_2^2$$

where  $P_0$  and  $N_0$  are constants, and  $\eta_1$ ,  $\eta_2$ ,  $\zeta_1$  and  $\zeta_2$  are four different centered random gaussian variables. Therefore, the fluctuation  $\Delta u_r$  of the longitudinal velocity difference can be written as

$$\Delta u_p = \psi_1(\mathbf{r}) \xi + \psi_2(\mathbf{r}) (\chi(\eta^2 - 1) - (\zeta^2 - 1)) \quad (50)$$

where  $\xi$ ,  $\eta$  and  $\zeta$  are independent centered random variables which have gaussian distribution functions with standard deviation equal to the unity. The parameter  $\chi$  is a positive definite function of Reynolds number, whereas  $\psi_1$  and  $\psi_2$  are functions of space coordinates and the Reynolds number.

At the Kolmogorov scale  $\ell$ , the order of magnitude of the velocity fluctuations is  $u_K^2 \tau / \ell$ , with  $\tau = 1/\Lambda$  and  $u_K = \nu/\ell$ , whereas  $\psi_2$  is negligible because is due to the inertia forces: this immediately identifies  $\psi_1 \approx u_K^2 \tau / \ell$ .

On the contrary, at the Taylor scale  $\lambda_T$ ,  $\psi_1$  is negligible and the order of magnitude of the velocity fluctuations is  $u^2 \tau / \lambda_T$ , therefore  $\psi_2 \approx u^2 \tau / \lambda_T$ .

The ratio  $\psi_2/\psi_1$  is a function of  $R_\lambda$

$$\psi(\mathbf{r}, R_\lambda) = \frac{\psi_2(\mathbf{r})}{\psi_1(\mathbf{r})} \approx \frac{u^2 \ell}{u_K^2 \lambda_T} = \sqrt{\frac{R_\lambda}{15\sqrt{15}}} \hat{\psi}(\mathbf{r}) \quad (51)$$

where  $\hat{\psi}(\mathbf{r}) = O(1)$ , is a function which has to be determined.

Hence, the dimensionless longitudinal velocity difference  $\Delta u_r$ , is written as

$$\frac{\Delta u_r}{\sqrt{\langle (\Delta u_r)^2 \rangle}} = \frac{\xi + \psi(\chi(\eta^2 - 1) - (\zeta^2 - 1))}{\sqrt{1 + 2\psi^2(1 + \chi^2)}} \quad (52)$$

The dimensionless statistical moments of  $\Delta u_r$  are easily calculated considering that  $\xi$ ,  $\eta$  and  $\zeta$  are independent gaussian variables

$$H_n \equiv \frac{\langle (\Delta u_r)^n \rangle}{\langle (\Delta u_r)^2 \rangle^{n/2}} = \frac{1}{(1 + 2\psi^2(1 + \chi^2))^{n/2}} \sum_{k=0}^n \binom{n}{k} \psi^k \langle \xi^{n-k} \rangle \langle (\chi(\eta^2 - 1) - (\zeta^2 - 1))^k \rangle \quad (53)$$

where

$$\begin{aligned} \langle (\chi(\eta^2 - 1) - (\zeta^2 - 1))^k \rangle &= \sum_{i=0}^k \binom{k}{i} (-\chi)^i \langle (\zeta^2 - 1)^i \rangle \langle (\eta^2 - 1)^{k-i} \rangle \\ \langle (\eta^2 - 1)^i \rangle &= \sum_{l=0}^i \binom{i}{l} (-1)^l \langle \eta^{2(i-l)} \rangle \end{aligned} \quad (54)$$

In particular, the third moment or skewness,  $H_3$ , which is responsible for the energy cascade, is

$$H_3 = \frac{8\psi^3(\chi^3 - 1)}{(1 + 2\psi^2(1 + \chi^2))^{3/2}} \quad (55)$$

For  $\chi \neq 1$ , the skewness and all the odd order moments are different from zero, and for  $n > 3$ , all the absolute moments are rising functions of  $R_\lambda$ , thus  $\Delta u_r$  exhibits an intermittency whose entity increases with the Reynolds number.

All the statistical moments can be calculated once the function  $\chi(R_\lambda)$  and the value of  $\hat{\psi}_0$  are known. The expression of  $K(r)$  obtained in the first part of the work allows to identify  $H_3(0)$  and then fixes the relationship between  $\psi_0$  and  $\chi(R_\lambda)$

$$-H_3(0) = \frac{8\psi_0^3(1 - \chi^3)}{(1 + 2\psi_0^2(1 + \chi^2))^{3/2}} = \frac{3}{7} \quad (56)$$

where  $\psi_0 = \psi(0, R_\lambda) = O(\sqrt{R_\lambda})$  and  $\chi = \chi(R_\lambda) > 0$ . This relationship does not admit solutions with  $\chi > 0$  below a minimum value of  $(R_\lambda)_{min}$  dependent on  $\hat{\psi}_0$ . According to the analysis of section 10 (Appendix B),  $(R_\lambda)_{min}$  is chosen to 10.12, which corresponds to  $\hat{\psi}_0 \simeq 1.075$ . (setting  $\chi = 0$ ,  $R_\lambda = 10.12$  in  $H_3(0)$ ). Varying the value of  $(R_\lambda)_{min}$  from 8.5 to 15 would bring values of  $\hat{\psi}_0$  between 1.2 and 0.9, respectively. In figure 2, the function  $\chi(R_\lambda)$  is shown for  $\hat{\psi}_0 = 1.075$ . The limit  $\chi \simeq 0.86592$  for  $R_\lambda \rightarrow \infty$  is reached independently of the value of  $\hat{\psi}_0$ .

The PDF of  $\Delta u_r$  is expressed through the Frobenius-Perron equation

$$F(\Delta u'_r) = \int_{\xi} \int_{\eta} \int_{\zeta} p(\xi)p(\eta)p(\zeta) \delta(\Delta u'_r - \Delta u_r(\xi, \eta, \zeta)) d\xi d\eta d\zeta \quad (57)$$

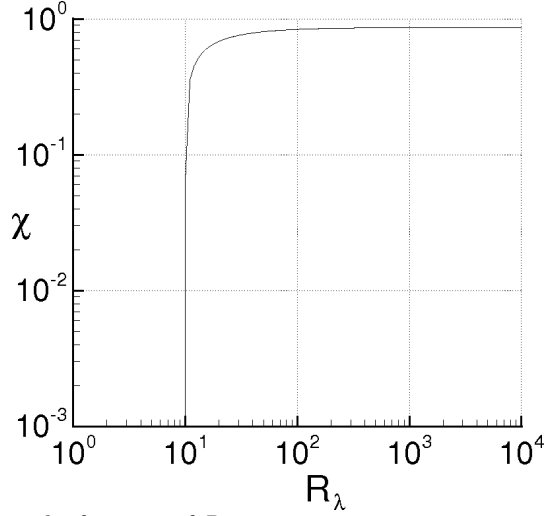


**Fig. 2** Parameter  $\chi$  plotted as the function of  $R_\lambda$ .

where  $\Delta u_r$  is calculated with Eq. (52),  $\delta$  is the Dirac delta and  $p$  is a gaussian PDF whose average value and standard deviation are equal to 0 and 1, respectively.

For non-isotropic turbulence or in more complex cases with boundary conditions, the velocity spectrum could not satisfy the Lindeberg condition, thus the velocity will be not distributed following a Gaussian PDF, and Eq. (50) changes its analytical form and can incorporate more intermittent terms [12] which give the deviation with respect to the isotropic turbulence. Hence, the absolute statistical moments of  $\Delta u_r$  will be greater than those calculated with Eq. (52), indicating that, in a more complex situation than the isotropic turbulence, the intermittency of  $\Delta u_r$  can be significantly stronger.

## 7 Results and discussion

In order to obtain informations about the validity of the proposed analysis, several results are now presented.

As the first result, the evolution in time of the correlation function is calculated with the proposed closure of the von Kármán-Howarth equation (Eq. (41)), where the boundary conditions are given by Eq. (71). The turbulent kinetic energy and the spectrums  $E(\kappa)$  and  $T(\kappa)$  are calculated with Eq. (72) and Eqs. (73), respectively. The calculation is carried out for the initial Reynolds number of  $Re = u(0)L_r/\nu = 2000$ , where  $L_r$  and  $u(0)$  are, respectively, the characteristic dimension of the problem and the initial velocity standard deviation. The initial condition for the correlation function is  $f(r) = \exp(-(r/\lambda_T)^2)$ , where  $\lambda_T/L_r = 1/(2\sqrt{2})$ , whereas  $u(0) = 1$ . The dimensionless time of the problem is defined as  $t = t u(0)/L_r$ .

Equation (67) was numerically solved adopting the Crank-Nicholson integrator scheme with variable time step, where the discretization of the space domain is made by  $N-1$  intervals of the same amplitude  $\Delta r$ . This corresponds to a discretization of the Fourier space made by  $N-1$  subsets in the interval  $[0, \kappa_M]$ , where  $\kappa_M = \pi/(2\Delta r)$ . For the adopted initial Reynolds number, the choice  $N = 1500$ , gives an adequate discretization, which provides  $\Delta r < \ell$ , for the whole simulation. For what concerns  $u$ , it was calculated with Eq. (72) and the kinetic energy was checked to be equal to the integral over  $\kappa$  of the energy spectrum. During the simulation,  $T(\kappa)$  must identically satisfy Eq.(74) (see Appendix A) which states that  $T(\kappa)$  does not modify the kinetic energy. According to the discretization of the Fourier space, the integral of  $T(\kappa)$  is calculated with the trapezes rule from 0 until to  $\kappa_M$ , at each time step, therefore, the simulation will be considered to be accurate as long as

$$\int_0^{\kappa_M} T(\kappa) d\kappa \simeq \int_0^\infty T(\kappa) d\kappa = 0 \quad (58)$$

namely, when  $T(\kappa) \simeq 0$  for  $\kappa > \kappa_M$ . As the simulation advances, according to Eq. (41), the energy cascade determines variations of  $E(\kappa)$  and  $T(\kappa)$  for wave-numbers whose values rise with the time,

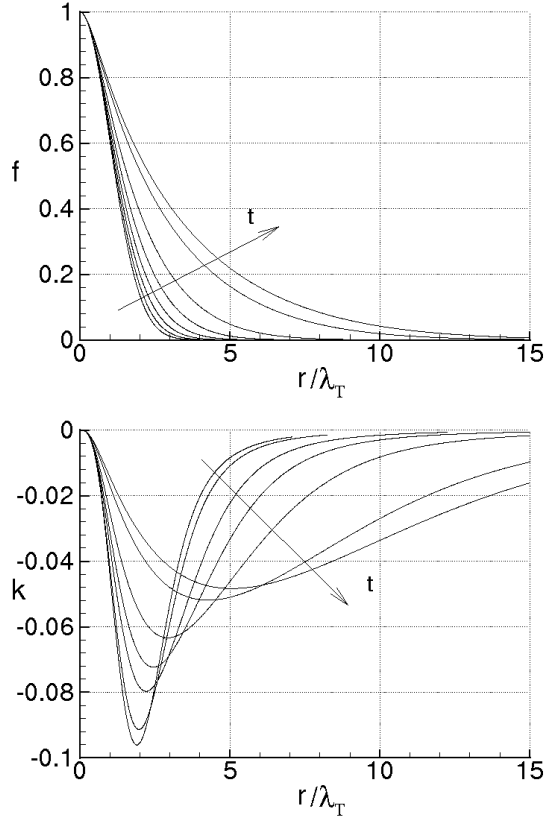


**Fig. 3** Correlation functions,  $f$  and  $k$  versus the separation distance at the times of simulation  $\bar{t} = 0, 0.1, 0.2, 0.3, 0.4, 0.5, 0.6, 0.63$ .

then Eq. (58) holds until to a certain time, where these wave-number are about equal to  $\kappa_M$ . At higher times, the variations of  $T(\kappa)$  can occur for  $\kappa > \kappa_M$ , out of the interval  $(0, \kappa_M)$ , thus Eq. (58) could be not satisfied. For this reason, the simulation is stopped as soon as the following condition is achieved [18]

$$\left| \int_0^{\kappa_M} T(\kappa) d\kappa \right| > \frac{1}{N^2} \int_0^{\kappa_M} |T(\kappa)| d\kappa \quad (59)$$

At the end of several simulations, we obtain  $\Delta r \approx 0.8 \ell$ , and, in this situation, the energy spectrum is here supposed to be fully developed.

The diagrams of Fig. 3 show the correlation functions  $f(r)$  and  $k(r)$  vs. the dimensionless distance  $r/\lambda_T$ , at different times of simulation. The kinetic energy and Taylor scale vary according to Eqs. (41) and (72), thus  $f(r)$  and  $k(r)$  change in such a way that the length scales associated to their variations diminish as the time increases, whereas the maximum of  $|k|$  decreases. At the final instants of the simulation, one obtains that  $f - 1 = O(r^{2/3})$  for  $r/\lambda_T = O(1)$ , whereas the maximum of  $|k|$  is about 0.05. These results are in very good agreement with the numerous data of the literature [8] which concern the evolution of correlation functions. Figure 4 shows the diagrams of  $E(\kappa)$  and  $T(\kappa)$  for the same times, where the dashed line in the plot of  $E(\kappa)$ , represents the  $-5/3$  Kolmogorov law [6]. The spectrums  $E(\kappa)$  and  $T(\kappa)$  vary with time according to Eqs. (41) and (73) and depend on the initial condition. At the end of simulation, the energy spectrum  $E(\kappa)$  can be compared with the dashed line in an opportune interval of wave-numbers. This arises from the developed correlation function, which behaves like  $f - 1 = O(r^{2/3})$  for  $r = O(\lambda_T)$ .

Next, the Kolmogorov function  $Q(r)$  and Kolmogorov constant  $C$ , are determined with the proposed analysis, using the previous results of the simulation.

Following the Kolmogorov theory, the Kolmogorov function, which is defined as

$$Q(r) = -\frac{\langle (\Delta u_r)^3 \rangle}{r\varepsilon} \quad (60)$$

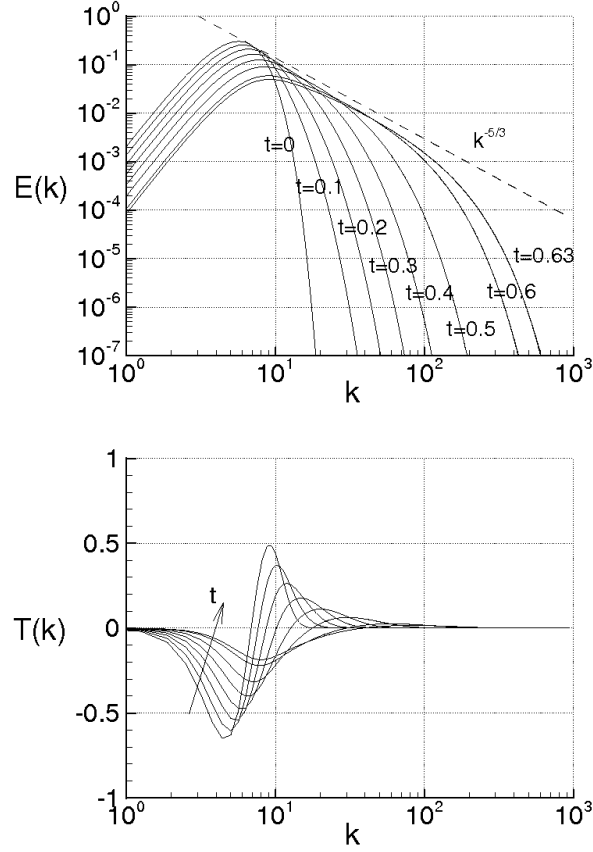


**Fig. 4** Plot of  $E(\kappa)$  and  $T(\kappa)$  at the diverse times of simulation.

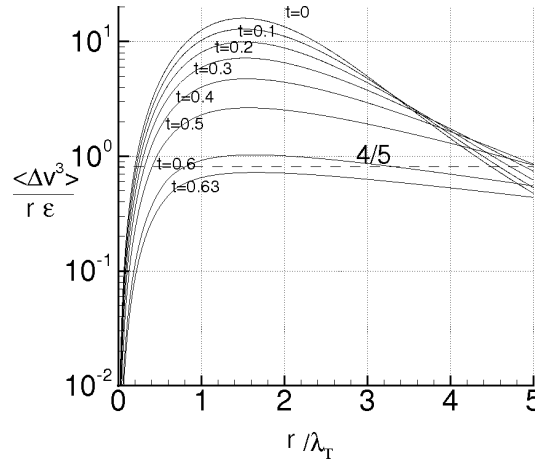


**Fig. 5** The Kolmogorov function versus  $r/\lambda_T$  for different times of simulation. The dashed line indicates the value  $4/5$ .

is constant with respect to  $r$ , and is equal to  $4/5$  as long as  $r/\lambda_T = O(1)$ . As shown in Fig. 5, for  $\bar{t} = 0$ , the maximum of  $Q(r)$  is much greater than  $4/5$  and its variations with  $r/\lambda_T$  can not be neglected. This is the consequence of the choice of the initial correlation function. At the successive times, the maximum of  $Q(r)$  decreases until to the final instants, where, with the exception of  $r/\lambda_T \approx 0$ ,  $Q(r)$  exhibits variations which are less than those calculated at the previous times in a wide range of  $r/\lambda_T$ , with a maximum which can be compared to  $0.8$ .

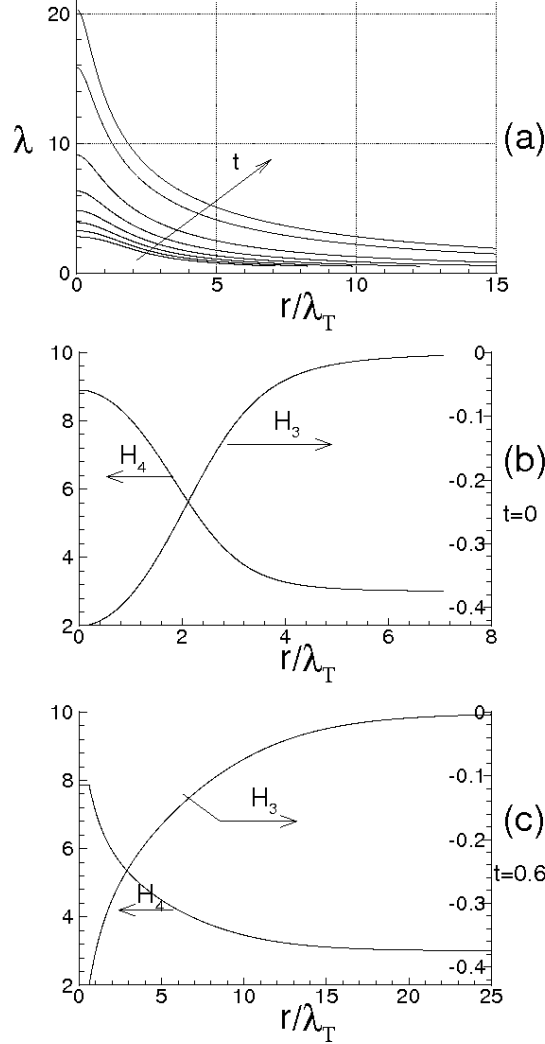


**Fig. 6** (a) Maximum finite size Lyapunov exponent at the times of simulation  $\bar{t} = 0, 0.1, 0.2, 0.3, 0.4, 0.5, 0.6, 0.63$ ; (b) and (c) skewness and Flatness versus  $r/\lambda_T$  at  $t = 0$  and  $t = 0.6$ , respectively.

The Kolmogorov constant  $C$  is also calculated by definition

$$E(\kappa) = C \frac{\varepsilon^{2/3}}{\kappa^{5/3}} \quad (61)$$

This is here determined, as the value of  $C$  which makes the curve represented by Eq. (61) to be tangent to the energy spectrum  $E(\kappa)$  previously calculated. At end simulation,  $C \simeq 1.932$ , namely  $C$  and  $Q_{max}$  agree with the corresponding quantities known from the literature.

For the same simulation, Fig. 6a shows the maximal finite scale Lyapunov exponent, calculated with Eq. (40), where  $\lambda$  varies according to  $f$ . For  $t = 0$ , the variations of  $\lambda$  are the result of the adopted initial correlation function which is a gaussian, whereas as the time increases, the variations of  $f$  determine sizable increments of  $\lambda$  and of its slope in proximity of the origin. Then, for developed spectrum, since  $f - 1 = O(r^{2/3})$ , the maximal finite scale Lyapunov exponent behaves like  $\lambda \approx r^{-2/3}$ . Thus, the diffusivity coefficient associated to the relative motion between two fluid particles, defined as  $D(r) \propto \lambda r^2$ , here satisfies the famous Richardson scaling law  $D(r) \approx r^{4/3}$ [5].

In the diagrams of Figs. 6b and 6c, skewness and flatness of  $\Delta u_r$  are shown in terms of  $r$  for  $\bar{t} = 0$  and  $0.6$ . The skewness,  $H_3$  is first calculated with Eq. (42), then  $H_4$  has been determined using Eq. (53). At  $\bar{t} = 0$ ,  $|H_3|$  starts from  $3/7$  at the origin with small slope, then decreases until to reach small values.  $H_4$  also exhibits small derivatives near the origin, where  $H_4 \gg 3$ , thereafter it decreases

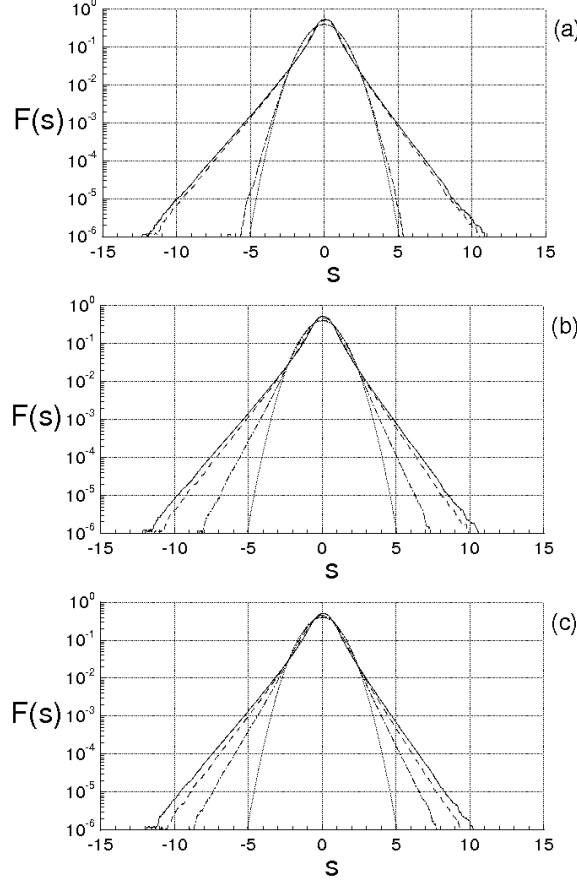


**Fig. 7** PDF of the velocity difference fluctuations at the times  $\bar{t}=0$  (a),  $\bar{t}=0.5$  (b) and  $\bar{t}=0.6$  (c). Continuous lines are for  $r=0$ , dashed lines are for  $r/\lambda_T=1$ , dot-dashed lines are for  $r/\lambda_T=5$ , dotted lines are for gaussian PDF.

more rapidly than  $|H_3|$ . At  $\bar{t}=0.6$ , the diagram importantly changes and exhibits different shapes. The Taylor scale and the corresponding Reynolds number are both changed, so that the variations of  $H_3$  and  $H_4$  are associated to smaller distances, whereas the flatness at the origin is slightly less than that at  $t=0$ . Nevertheless, these variations correspond to higher  $r/\lambda_T$  than those for  $t=0$ , and also in this case,  $H_4$  reaches the value of 3 more rapidly than  $H_3$  tends to zero.

The PDFs of  $\Delta u_r$  are calculated with Eqs. (57) and (52), and are shown in Fig. 7 in terms of the dimensionless abscissa

$$s = \frac{\Delta u_r}{\langle (\Delta u_r)^2 \rangle^{1/2}}$$

where, these distribution functions are normalized, in order that their standard deviations are equal to the unity. The figure represents the distribution functions of  $s$  for several  $r/\lambda_T$ , at  $\bar{t}=0, 0.5$  and  $0.6$ , where the dotted curves represent the gaussian distribution functions. The calculation of  $H_3(r)$  is first carried out with Eq. (42), then the function  $\psi(r, R_\lambda)$  is identified through Eq. (55), and finally the PDF is obtained with Eq. (57). For  $t=0$  (see Fig. 7a) and according to the evolutions of  $H_3$  and  $H_4$ , the PDFs calculated at  $r/\lambda_T=0$  and  $1$ , are quite similar each other, whereas for  $r/\lambda_T=5$ , the PDF is almost a gaussian function. Toward the end of the simulation, (see Fig. 7b and c), the two PDFs calculated at  $r/\lambda_T=0$  and  $1$ , exhibit more sizable differences, whereas for  $r/\lambda_T=5$ , the PDF differs very much from a gaussian PDF. This is in line with the plots of  $H_3(r)$  and  $H_4(r)$  of Fig. 6.

Next, the spatial structure of  $\Delta u_r$ , given by Eq. (52), is analyzed using the previous results of the simulation. According to the various works [19], [20],  $\Delta u_r$  behaves quite similarly to a multifractal system, where  $\Delta u_r$  obeys to a law of the kind  $\Delta u_r(r) \approx r^q$  where the exponent  $q$  is a fluctuating

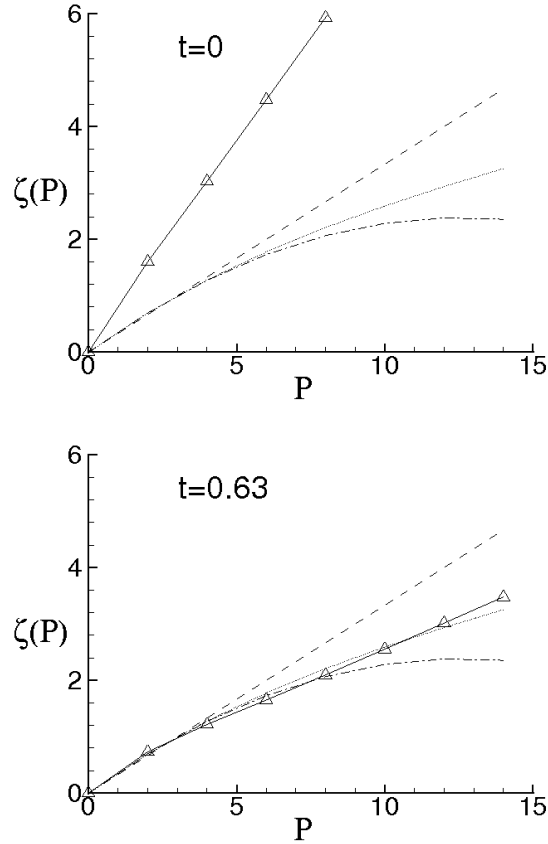


**Fig. 8** Scaling exponents of longitudinal velocity difference versus the order moment at different times. Continuous lines with solid symbols are for the present data. Dashed lines are for Kolmogorov K41 data [6]. Dashdotted lines are for Kolmogorov K62 data [19]. Dotted lines are for She-Leveque data [20]

function of space. This implies that the statistical moments of  $\Delta u_r(r)$  are expressed through different scaling exponents  $\zeta(P)$  whose values depend on the moment order  $P$ , i.e.

$$\langle (\Delta u_r)^P(r) \rangle = A_P r^{\zeta(P)} \quad (62)$$

These scaling exponents are here identified through a best fitting procedure, in the interval  $(a, a + \lambda_T)$ , where the endpoints  $a$  is an unknown quantity which has to be determined. The location of this interval varies with the time. The calculation of  $a$  and of  $\zeta_P$  and  $A_P$  is carried out through a minimum square method which for each moment order is applied to the following optimization problem

$$J_P(\zeta_P, A_P) \equiv \int_a^{a+\lambda_T} (\langle (\Delta u_r)^P \rangle - A_P r^{\zeta(P)})^2 dr = \min, \quad P = 1, 2, \dots \quad (63)$$

where  $\langle (\Delta u_r)^P \rangle$  are calculated with Eqs. (53), and  $a$  is calculated in order to obtain  $\zeta(3) = 1$ .

Figure 8 shows the comparison between the scaling exponents here obtained (continuous lines with solid symbols) and those of the Kolmogorov theories K41 [6] (dashed lines) and K62 [19] (dashdotted lines), and those given by She-Leveque [20] (dotted curves). At  $t = 0$ , the values of  $\zeta(P)$  are the result of the chosen initial condition. As the time increases, the correlation function changes causing variations in the statistical moments of  $\Delta u_r(r)$ . As result,  $\zeta(P)$  gradually diminish and exhibit a variable slope

**Table 1** Scaling exponents of the longitudinal velocity difference.

P	1	2	3	4	5	6	7	8	9	10	11	12	13	14
$\zeta(P)$	0.36	0.71	1.00	1.19	1.41	1.61	1.84	2.04	2.25	2.49	2.72	2.93	3.15	3.38

which depends on the moment order  $P$ , until to reach the situation of Fig. 8b, where the simulation is just ended. The dimensionless moments of  $\Delta u_r(r)$  are changed. The plot of  $\zeta(P)$  shows that near the origin,  $\zeta(P) \simeq P/3$ , and that the values of  $\zeta(P)$  seem to be in agreement with the those proposed by She-Leveque. More in detail, Table I reports these scaling exponents in terms of the moments order, calculated for  $\bar{t} = 0.63$ . These values are the consequence of the spatial variations of the skewness, calculated using Eq. (42), and of the quadratic terms due to the inertia and pressure forces into the expression of the velocity difference, which make  $\langle (\Delta u_r)^P \rangle$  a quantity quite similar to a multifractal system.

Other simulations with different initial correlation functions and Reynolds numbers have been carried out, and all of them lead to analogous results, in the sense that, at the end of the simulations, the diverse quantities such as  $Q(r)$ ,  $C$  and  $\zeta(P)$  are quite similar to those just calculated. For what concerns the effect of the Reynolds number, its increment determines a wider range of the wave-numbers where  $E(\kappa)$  is comparable with the Kolmogorov law and a smaller dissipation energy rate in accordance to Eq. (72).

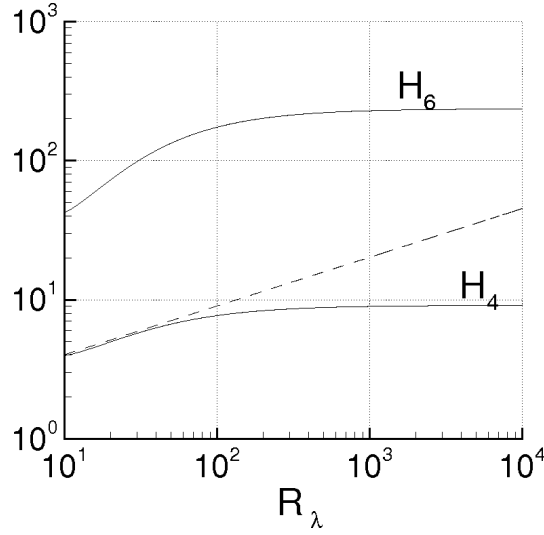
In order to study the evolution of the intermittency vs. the Reynolds number, Table II gives the first ten statistical moments of  $F(\partial u_r / \partial r)$ . These are calculated with Eqs. (53) and (54), for  $R_\lambda = 10, 12, 100$  and  $1000$ , and are shown in comparison with those of a gaussian distribution function. It is apparent that a constant nonzero skewness of the longitudinal velocity derivative, causes an intermittency which rises with  $R_\lambda$  (see Eq. (52)). More specifically, Fig. 9 shows the variations of  $H_4(0)$  and  $H_6(0)$  (continuous lines) in terms of  $R_\lambda$ , calculated with Eqs. (53) and (54), with  $H_3(0) = -3/7$ . These moments are rising functions of  $R_\lambda$  for  $10 < R_\lambda < 700$ , whereas for higher  $R_\lambda$  these tend to the saturation and such behavior also happens for the other absolute moments. According to Eq. (53), in the interval  $10 < R_\lambda < 70$ ,  $H_4$  and  $H_6$  result to be about proportional to  $R_\lambda^{0.34}$  and  $R_\lambda^{0.78}$ , respectively, and the intermittency increases with the Reynolds number until to  $R_\lambda \approx 700$ , where it ceases to rise so quickly. This behavior, represented by the continuous lines, depends on the fact that  $\psi \approx \sqrt{R_\lambda}$ , and results to be in very good agreement with the data of Pullin and Saffman [21], for  $10 < R_\lambda < 100$ .

Figure 9 can be compared with the data collected by Sreenivasan and Antonia [16], which are here reported into Fig. 10. These latter are referred to several measurements and simulations obtained in different situations which can be very far from the isotropy and homogeneity conditions. Nevertheless a comparison between the present results and those of Ref. [16] is an opportunity to state if the two data exhibit elements in common. According to Ref. [16], the flatness monotonically rises with  $R_\lambda$  with a rising rate which agrees with Eq. (54) for  $10 < R_\lambda < 60$  (dashed line, Fig. 9), whereas the skewness seems to exhibit minor variations. Thereafter,  $H_4$  continues to rise with about the same rate, without the saturation observed in Fig. 9. The weaker intermittency calculated with the present analysis arise from the isotropy which makes the velocity fluctuation a gaussian random variable, while, as seen in sec. 6, without the isotropy condition, the flatness of velocity and of velocity difference can be much greater than that of the isotropic case.

Again, the obtained results are compared with the data of Tabeling *et al* [14], [15], where, in an experiment using low temperature helium gas between two counter-rotating cylinders (closed cell), the authors measure the PDF of  $\partial u_r / \partial r$  and its moments. Also in this case the flow can be quite far from to the isotropy condition. In fact, these experiments pertain wall-bounded flows, where the walls could importantly influence the fluid velocity in proximity of the probe. The authors found that the higher moments than the third order, first increase with  $R_\lambda$  until to  $R_\lambda \approx 700$ , then exhibit a lightly

**Table 2** Dimensionless statistical moments of  $F(\partial u_r / \partial r)$  at different Taylor scale Reynolds numbers. P.R. as for "present results".

Moment Order	$R_\lambda \approx 10$ P. R.	$R_\lambda = 10^2$ P. R.	$R_\lambda = 10^3$ P. R.	Gaussian Moment
3	-.428571	-.428571	-.428571	0
4	3.96973	7.69530	8.95525	3
5	-7.21043	-11.7922	-12.7656	0
6	42.4092	173.992	228.486	15
7	-170.850	-551.972	-667.237	0
8	1035.22	7968.33	11648.2	105
9	-6329.64	-41477.9	-56151.4	0
10	45632.5	617583.	997938.	945



**Fig. 9** Dimensionless moments  $H_4(0)$  and  $H_6(0)$  plotted vs.  $R_\lambda$ . Continuous lines are for the present results. The dashed line is the tangent to the curve of  $H_4(0)$  in  $R_\lambda \approx 10$ .

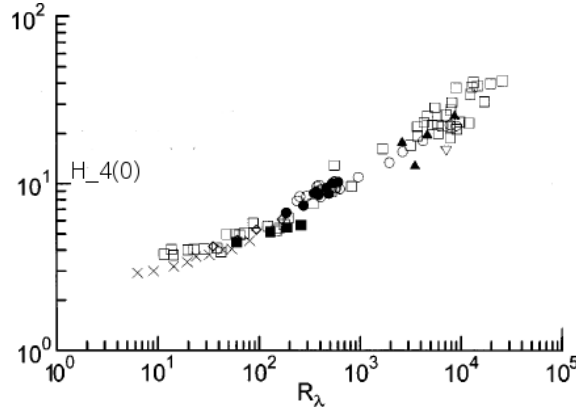


**Fig. 10** Flatness  $H_4(0)$  vs.  $R_\lambda$ . These data are from Ref.[16].

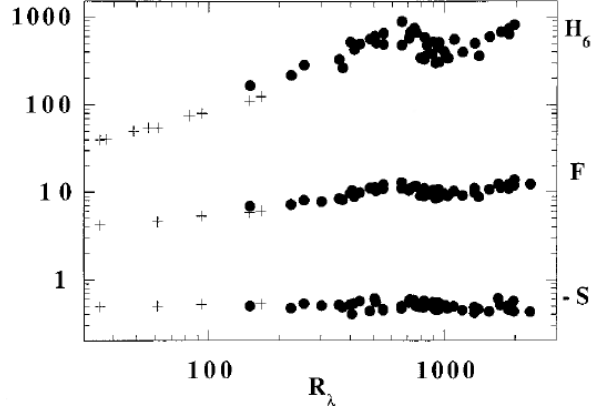
non-monotonic evolution with respect to  $R_\lambda$ , and finally cease their variations denoting a transition behavior (See Fig. 11). As far as the skewness is concerned, the authors observe small percentage variations. Although the isotropy does not describe the non-monotonic evolution near  $R_\lambda = 700$ , the results obtained with Eq. (52) can be considered comparable with those of Refs. [14], [15], resulting also in this case, that the proposed analysis gives a weaker intermittency with respect to Refs. [14], [15].

The normalized PDFs of  $\partial u_r / \partial r$  are calculated with Eqs. (57) and (52), and are shown in Fig. 12 in terms of the variable  $s$ , which is defined as

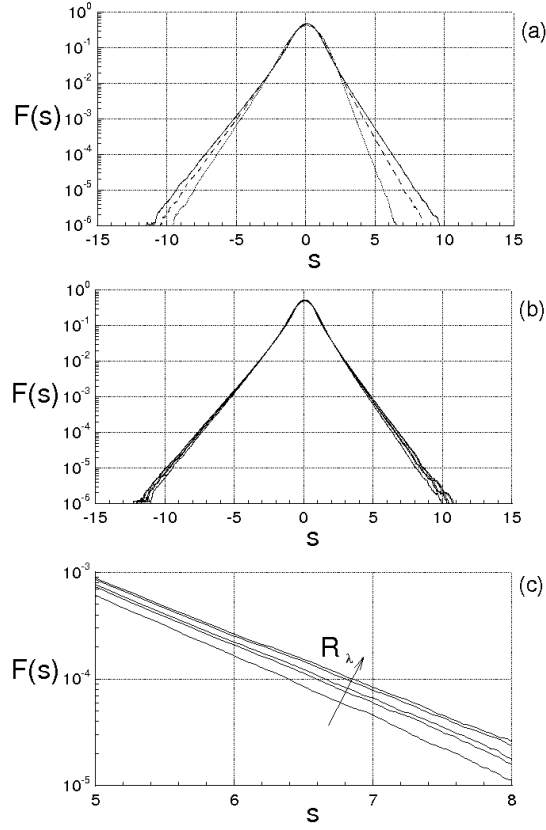
$$s = \frac{\partial u_r / \partial r}{\langle (\partial u_r / \partial r)^2 \rangle^{1/2}}$$

Figure 12a shows the diagrams for  $R_\lambda = 15, 30$  and  $60$ , where the PDFs vary in such a way that  $H_3(0) = -3/7$ .

As well as in Ref. [15], Figs. 4b and 4c give the PDF for  $R_\lambda = 255, 416, 514, 1035$  and  $1553$ , where these last Reynolds numbers are calculated through the Kolmogorov function given in Ref. [15], with  $H_3(0) = -3/7$ . In particular, Fig. 12c represents the enlarged region of Fig. 12b, where the tails of PDF are shown for  $5 < s < 8$ . According to Eq. (52), the tails of the PDF rise in the interval  $10 < R_\lambda < 700$ , whereas at higher  $R_\lambda$ , smaller variations occur. Although the non-monotonic trend observed in Ref. [15], Fig. 12c shows that the values of the PDFs calculated with the proposed analysis, for  $5 < s < 8$ ,



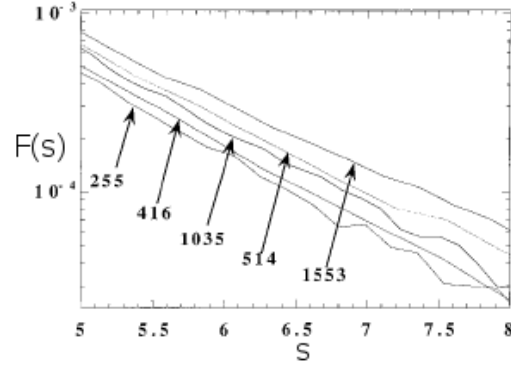
**Fig. 11** Skewness  $S = H_3(0)$ , Flatness  $F = H_4(0)$  and hyperflatness  $H_6(0)$  vs.  $R_\lambda$ . These data are from Ref.[15].



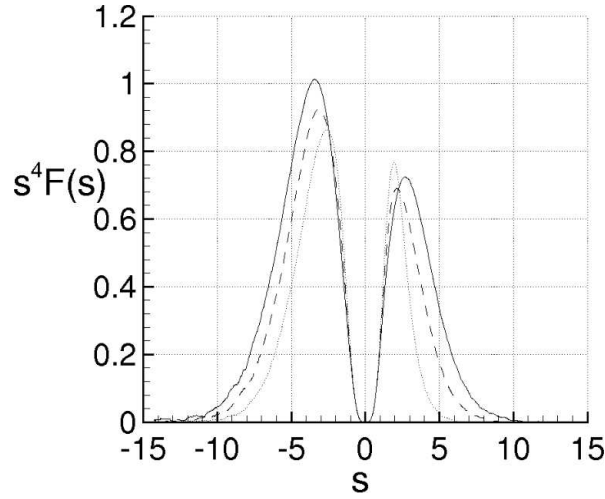
**Fig. 12** Log linear plot of the PDF of  $\partial u_r / \partial r$  for different  $R_\lambda$ . (a): dotted, dashdotted and continuous lines are for  $R_\lambda = 15, 30$  and  $60$ , respectively. (b) and (c) PDFs for  $R_\lambda = 255, 416, 514, 1035$  and  $1553$ . (c) represents an enlarged part of the diagram (b)

exhibit the same order of magnitude of those obtained by Tabeling *et al* [15] which are here shown in Fig. 13.

Asymmetry and intermittency of the distribution functions are also represented through the integrand function of the 4<sup>th</sup> order moment of PDF, which is  $J_4(s) = s^4 F(s)$ . This function is shown in terms of  $s$ , in Fig. 14, for  $R_\lambda = 15, 30$  and  $60$ .



**Fig. 13** PDF of  $\partial u_r / \partial r$  for  $R_\lambda = 255, 416, 514, 1035$  and  $1553$ . These data are from Ref. [15]



**Fig. 14** Plot of the integrand  $s^4 F(s)$  for different  $R_\lambda$ . Dotted, dashdotted and continuous lines are for  $R_\lambda = 15, 30$  and  $60$ , respectively.

## 8 Conclusions

The proposed analysis is based on the conjecture which states that the turbulence is caused by the bifurcations of the velocity field. The main limitation of this analysis is that it only studies the developed homogeneous-isotropic turbulence, whereas this does not consider the intermediate stages of the turbulence.

The results of this analysis can be here summarized:

1. The momentum equations written using the referential coordinates allow to factorize the velocity fluctuation and to express it in Lyapunov exponential form of the local fluid deformation. As a result, the velocity fluctuation is the combined effect of the exponential growth rate and of the rotations of the Lyapunov basis with respect to the fixed frame of reference.
2. The finite scale Lyapunov analysis of the relative motion provides an explanation of the physical mechanism of the energy cascade in turbulence and gives a closure of the von Kármán-Howarth equation.

The fluid incompressibility determines that the inertia forces transfer the kinetic energy between the length scales without changing the total kinetic energy. This implies that the skewness of the longitudinal velocity derivative is a constant of the present analysis and that the energy cascade mechanism does not depend on the Reynolds number.

3. The statistics of  $\Delta u_r$  can be inferred looking at the Fourier series of the velocity difference. This is a non-Gaussian statistics, where the constant skewness of  $\partial u_r / \partial r$  implies that the other higher absolute moments increase with the Taylor-scale Reynolds number.
4. The closure of the von Kármán-Howarth equation, shows that the mechanism of energy cascade gives energy spectrums that can be compared with the Kolmogorov law  $\kappa^{-5/3}$  in an opportune range of wave-numbers.
5. For developed energy spectrums, the Kolmogorov function exhibits, in an opportune range of  $r$ , small variations much less than at the previous times, and its maximum is quite close to  $4/5$ , whereas the Kolmogorov constant is about equal to 1.93. As the consequence, the maximal finite scale Lyapunov exponent and the diffusivity coefficient vary according to the Richardson law when the separation distance is of the order of the Taylor scale.
6. The analysis also determines the scaling exponents of the moments of the longitudinal velocity difference through a best fitting procedure. For developed energy spectrum, these exponents show variations with the moment order which seem to be consistent with those known from the literature.

**Acknowledgements** This work was partially supported by the Italian Ministry for the Universities and Scientific and Technological Research (MIUR). The author would like to thank prof. Luciano M. de Socio for his useful comments.

## 9 Appendix A

The von Kármán-Howarth equation gives the evolution in time of the longitudinal correlation function for isotropic turbulence. The correlation function of the velocity components is the symmetrical second order tensor  $R_{ij}(\mathbf{r}) = \langle u_i u'_j \rangle$ , where  $u_i$  and  $u'_j$  are the velocity components at  $\mathbf{x}$  and  $\mathbf{x} + \mathbf{r}$ , respectively, being  $\mathbf{r}$  the separation vector. The equations for  $R_{ij}$  are obtained by the Navier-Stokes equations written in the two points  $\mathbf{x}$  and  $\mathbf{x} + \mathbf{r}$  [7], [8]. For isotropic turbulence  $R_{ij}$  can be expressed as

$$R_{ij}(\mathbf{r}) = u^2 \left[ (f - g) \frac{r_i r_j}{r^2} + g \delta_{ij} \right] \quad (64)$$

$f$  and  $g$  are, respectively, longitudinal and lateral correlation functions, which are

$$f(r) = \frac{\langle u_r(\mathbf{x}) u_r(\mathbf{x} + \mathbf{r}) \rangle}{u^2}, \quad g(r) = \frac{\langle u_n(\mathbf{r}) u_n(\mathbf{x} + \mathbf{r}) \rangle}{u^2} \quad (65)$$

where  $u_r$  and  $u_n$  are, respectively, the velocity components parallel and normal to  $\mathbf{r}$ , whereas  $r = |\mathbf{r}|$  and  $u^2 = \langle u_r^2 \rangle = \langle u_n^2 \rangle = 1/3 \langle u_i u_i \rangle$ . Due to the continuity equation,  $f$  and  $g$  are linked each other by the relationship

$$g = f + \frac{1}{2} \frac{\partial f}{\partial r} r \quad (66)$$

The von Kármán-Howarth equation reads as follows [7], [8]

$$\frac{\partial f}{\partial t} = \frac{K}{u^2} + 2\nu \left( \frac{\partial^2 f}{\partial r^2} + \frac{4}{r} \frac{\partial f}{\partial r} \right) - 10\nu \frac{\partial^2 f}{\partial r^2}(0) f \quad (67)$$

where  $K$  is an even function of  $r$ , which is defined by the following equation [7], [8]

$$\left( r \frac{\partial}{\partial r} + 3 \right) K(r) = \frac{\partial}{\partial r_k} \langle u_i u'_i (u_k - u'_k) \rangle \quad (68)$$

and which can also be expressed as

$$K(r) = u^3 \left( \frac{\partial}{\partial r} + \frac{4}{r} \right) k(r) \quad (69)$$

where  $k$  is the longitudinal triple correlation function

$$k(r) = \frac{\langle u_r^2(\mathbf{x}) u_r(\mathbf{x} + \mathbf{r}) \rangle}{u^3} \quad (70)$$

The boundary conditions of Eq. (67) are [7], [8]

$$f(0) = 1, \quad \lim_{r \rightarrow \infty} f(r) = 0 \quad (71)$$

The viscosity is responsible for the decay of the turbulent kinetic energy, the rate of which is [7], [8]

$$\frac{du^2}{dt} = 10\nu u^2 \frac{\partial^2 f}{\partial r^2}(0) \quad (72)$$

This energy is distributed at different wave-lengths according to the energy spectrum  $E(\kappa)$  which is calculated as the Fourier Transform of  $fu^2$ , whereas the "transfer function"  $T(\kappa)$  is the Fourier Transform of  $K$  [8], i.e.

$$\left[ \frac{E(\kappa)}{T(\kappa)} \right] = \frac{1}{\pi} \int_0^\infty \left[ \frac{u^2 f(r)}{K(r)} \right] \kappa^2 r^2 \left( \frac{\sin \kappa r}{\kappa r} - \cos \kappa r \right) dr \quad (73)$$

where  $\kappa = |\boldsymbol{\kappa}|$  and  $T(\kappa)$  identically satisfies to the integral condition

$$\int_0^\infty T(\kappa) d\kappa = 0 \quad (74)$$

which states that  $K$  does not modify the total kinetic energy. The rate of energy dissipation  $\varepsilon$  is calculated for isotropic turbulence as follows [8]

$$\varepsilon = -\frac{3}{2} \frac{du^2}{dt} = 2\nu \int_0^\infty \kappa^2 E(\kappa) d\kappa \quad (75)$$

The microscales of Taylor  $\lambda_T$ , and of Kolmogorov  $\ell$ , are defined as

$$\lambda_T^2 = \frac{u^2}{\langle (\partial u_r / \partial r)^2 \rangle} = -\frac{1}{\partial^2 f / \partial r^2(0)}, \quad \ell = \left( \frac{\nu^3}{\varepsilon} \right)^{1/4} \quad (76)$$

## 10 Appendix B: Critical Reynolds number

The purpose of this appendix is to provide an estimation of the critical Reynolds number assuming that the turbulence is, in any case, fully developed, homogeneous and isotropic. Thus, the obtained results are subjected to these assumptions.

To this end, consider now the equation of motion of a fluid particle  $d\mathbf{x}/dt = \mathbf{u}(\mathbf{x}, t)$  and its fixed points which satisfy  $d\mathbf{x}/dt = 0$ . We assume that the bifurcations cascade of this equation are expressed in terms of the characteristic scales by the asymptotic approximation [11]

$$l_n = \frac{l_1}{\alpha^{n-1}} \quad (77)$$

where  $\alpha \approx 2$  [11], [22], and  $l_n$  represent the average distance between two branches of fixed points which born in the same bifurcation. Equation (77) is supposed to describe the route toward the chaos and is assumed to be valid until the onset of the turbulence. In this situation the minimum for  $l_n$  can not be less than the dissipation length or Kolmogorov scale  $\ell = (\nu^3/\varepsilon)^{1/4}$  [1], where  $l_1$  gives a good estimation of the correlation length of the phenomenon [11], [23] which, in this case is the Taylor scale  $\lambda_T$ . Thus,  $\ell < l_n < \lambda_T$ , and

$$\ell = \frac{\lambda_T}{\alpha^{N-1}} \quad (78)$$

where  $N$  is the number of bifurcations at the beginning of the turbulence. Equation (78) gives the connection between the critical Reynolds number and number of bifurcations. In fact, the characteristic Reynolds numbers associated to the scales  $\ell$  and  $\lambda_T$  are  $R_K = \ell u_K / \nu \equiv 1$  and  $R_\lambda = \lambda_T u / \nu$ , respectively, where  $u_K = (\nu \varepsilon)^{1/4}$  is characteristic velocity at the Kolmogorov scale, and  $u = \sqrt{\langle u_i u_i \rangle} / \sqrt{3}$  is the velocity standard deviation [8]. For isotropic turbulence, these scales are linked each other by [8]

$$\lambda_T / \ell = 15^{1/4} \sqrt{R_\lambda} \quad (79)$$

In view of Eq. (78), this ratio can be also expressed through  $N$ , i.e.

$$\alpha^{N-1} = 15^{1/4} \sqrt{R_\lambda} \quad (80)$$

Assuming that  $\alpha$  is equal to the Feigenbaum constant (2.502...), the value  $R_\lambda \simeq 1.6$  obtained for  $N = 2$  is not compatible with  $\lambda_T$  which is the correlation scale, while the result  $R_\lambda \simeq 10.12$ , calculated for  $N = 3$ , is an acceptable minimum value for  $R_\lambda$ . The order of magnitude of these values can be considered in agreement with the various scenarios describing the roads to the turbulence [24], [22], [25], [26], and with the diverse experiments [27], [28], [29] which state that the turbulence begins for  $N \geq 3$ . Of course, this minimum value for  $R_\lambda$  is the result of the assumptions  $\alpha \simeq 2.502$ ,  $l_1 \simeq \lambda_T$ ,  $l_N \simeq \ell$  and of the asymptotic approximation (77).

## References

1. LANDAU, L. D., LIFSHITZ, M., *Fluid Mechanics*. Pergamon London, England, 1959.
2. OTTINO, J. M., *The kinematics of mixing: stretching, chaos, and transport*, Cambridge Texts in Applied Mathematics, New York, 1989.
3. OTTINO, J. M., Mixing, Chaotic Advection, and Turbulence., *Annu. Rev. Fluid Mech.* **22**, 207–253, 1990.
4. TRUESDELL, C. *A First Course in Rational Continuum Mechanics*, Academic, New York, 1977.
5. RICHARDSON, L. F., Atmospheric Diffusion shown on a distance-neighbour graph., *Proc. Roy. Soc. London*, A **110**, 709, 1926.
6. KOLMOGOROV, A. N., Dissipation of Energy in Locally Isotropic Turbulence. Dokl. Akad. Nauk SSSR **32**, 1, 19–21, 1941.
7. VON KÁRMÁN, T. & HOWARTH, L., On the Statistical Theory of Isotropic Turbulence., *Proc. Roy. Soc. A*, **164**, 14, 192, 1938.
8. BATCHELOR, G.K., *The Theory of Homogeneous Turbulence*. Cambridge University Press, Cambridge, 1953.
9. LAMB, H. *Hydrodynamics*, Dover Publications, 1945.
10. CHRISTIANSEN, F., RUGH, H. H., Computing Lyapunov spectra with continuous Gram–Schmidt orthonormalization, *Nonlinearity*, Vol. 10, No. 5, pp. 1063–1072, 1997.
11. GUCKENHEIMER, J., HOLMES, P., *Nonlinear Oscillations, Dynamical Systems, and Bifurcations of Vector Fields*. Springer, 1990.
12. LEHMANN, E.L., *Elements of Large-sample Theory*. Springer, 1999.
13. A. I. BORISENKO, I. E. TARAPOV, *Vector and tensor analysis with applications*. Dover, 1990.
14. TABELING, P., ZOCCHI, G., BELIN, F., MAURER, J., WILLAIME, H., Probability density functions, skewness, and flatness in large Reynolds number turbulence, *Phys. Rev. E* **53**, 1613, 1996.
15. BELIN, F., MAURER, J., WILLAIME, H., TABELING, P., Velocity Gradient Distributions in Fully Developed Turbulence: An Experimental Study, *Physics of Fluid* **9**, no. 12, 3843–3850, 1997.
16. SREENIVASAN, K. R., ANTONIA, R. A., The Phenomenology of Small-Scale Turbulence., *Annu. Rev. Fluid Mech.* **29**, 435–472, 1997.
17. MADOW, W. G., Limiting Distributions of Quadratic and Bilinear Forms., *The Annals of Mathematical Statistics*, Vol. 11, No. 2, (Jun. 1940), 125–146, 1940.
18. HILDEBRAND, F.B., *Introduction to Numerical Analysis*, Dover Publications, 1987.
19. KOLMOGOROV, A. N., Refinement of Previous Hypothesis Concerning the Local Structure of Turbulence in a Viscous Incompressible Fluid at High Reynolds Number, *J. Fluid Mech.* **12**, 82–85, 1962.
20. SHE, Z.S. AND LEVEQUE, E., Universal scaling laws in fully developed turbulence, *Phys. Rev. Lett.* **72**, 336, 1994.
21. PULLIN, D., SAFFMAN, P., On the Lundgren Townsend model of turbulent fine structure, *Phys. Fluids*, A **5**, 1, 126, 1993.
22. FEIGENBAUM, M. J., *J. Stat. Phys.* **19**, 1978.
23. PRIGOGINE, I., *Time, Chaos and the Laws of Chaos*. Ed. Progress, Moscow, 1994.
24. RUELLE, D. & TAKENS, F., *Commun. Math. Phys.* **20**, 167, 1971.
25. POMEAU, Y., MANNEVILLE, P., *Commun. Math. Phys.* **74**, 189, 1980.
26. ECKMANN, J.P., Roads to turbulence in dissipative dynamical systems *Rev. Mod. Phys.* **53**, 643–654, 1981.
27. GOLLUB, J.P., SWINNEY, H.L., Onset of Turbulence in a Rotating Fluid., *Phys. Rev. Lett.* **35**, 927, 1975.
28. GIGLIO M., MUSAZZI S., PERINI U., Transition to chaotic behavior via a reproducible sequence of period doubling bifurcations, *Phys. Rev. Lett.* **47**, 243, 1981.
29. MAURER, J., LIBCHABER A., Rayleigh–Bénard Experiment in Liquid Helium: Frequency Locking and the onset of turbulence, *Journal de Physique Letters* **40**, L419–L423, 1979.